Soot and charcoal are reservoirs of extracellular DNA

S. Jelavić,[a,b*] L.G. Thygesen,[c] V. Magnin,[b] N. Findling,[b] S. Müller,[d] V. Meklesh,[e] K.K. Sand[a]

[a]Centre for Geogenetics, GLOBE Institute, University of Copenhagen, Øster Voldgade 5–7, 1350 Copenhagen, Denmark.

[b]Université Grenoble Alpes, Université Savoie Mont Blanc, CNRS, IRD, Université Gustave Eiffel, ISTerre, F-38000 Grenoble, France.

[c]University of Copenhagen, Department of Geoscience and Natural Resource Management, Rolighedsvej 23, 1958 Frederiksberg C, Denmark.

[d]University of Copenhagen, Department of Geosciences and Natural Resource Management, Øster Voldgade 10, 1350 Copenhagen K, Copenhagen, Denmark.

[e]Centre for Environmental and Climate Science, Lund University, Sölvegatan 37, 223 62 Lund, Sweden.

*corresponding author: stanislav.jelavic@univ-grenoble-alpes.fr

ABSTRACT

The vast potential of using sediment adsorbed DNA as a window to past and present biodiversity rely on the ability of solid surfaces to adsorb environmental DNA. However, a comprehensive insight into DNA adsorption at surfaces in general is lacking. Soot and charcoal are carbonaceous materials widespread in the environment where they readily can come in contact with extracellular DNA shed from organisms. Using batch adsorption, we measured DNA adsorption capacity at soot and charcoal as a function of solution composition, time and DNA length. We observed that the adsorption capacity for DNA is highest at low pH, that it increases with solution concentration and cation valency and that the activation energy for DNA adsorption at both soot and charcoal is ~50 kJmol^{-1}, suggesting strong binding. We demonstrate how the interaction between DNA and soot and charcoal partly occurs via terminal base pairs, suggesting that, besides electrostatic forces, hydrophobic interactions play an important role in binding. The large adsorption capacities and strong binding of DNA to soot and charcoal are features important for eDNA research and provide a motivation for use of carbonaceous materials from, e.g. anthropogenic pollution or wildfire as sources of biodiversity information.

INTRODUCTION

Environmental DNA (eDNA) is genetic information shed from living or deceased organisms into their surroundings. Free extracellular eDNA degrades in matter of days but when adsorbed to minerals in sediments, it can be preserved for thousands of years.[1,2] The adsorptive protection provided by minerals is likely a result of disrupted molecular recognition of adsorbed DNA by enzymes[3,4] and the inactivation of enzymes by adsorption to the same surfaces.[5] Once adsorbed, the eDNA can be transported across time and space following sedimentary processes. Consequently, mineral stored eDNA is a unique resource of information relevant for estimating past and present biodiversity,[6] monitoring of invasive and endangered species[7] and for reconstruction of paleoenvironments.[8] Given that eDNA can be extracted from water, sediments[9] and air,[10,11] the contribution of common non-

mineral environmental surfaces such as carbonaceous materials (CM) to the environmental reservoir of DNA is unclear.

CMs are produced anthropogenically and naturally by burning fossil fuels and vegetation. CMs are ubiquitous in soils and, because of their low density and small size, they are easily transported by air to aqueous environments including freshwater and marine sediments.[12] The abundance, easy transportation and widespread occurrence renders soot and charcoal as promising reservoirs of eDNA. Incomplete combustion of fossil fuels produces soot while burning of vegetation produces both charcoal by pyrolysis and soot by combustion and condensation of gases within fire. There is a great variability in structure and composition of soot and charcoal depending on their source materials and temperature of formation.[12,13] In general, both can be envisaged as polycyclic aromatic materials built from agglomerates of ordered graphitic domains consisting of sp^2-hybridised carbon and domains that deviate from a perfect graphitic structure with an increased incorporation of oxygen and hydrogen.[14–16] An important difference is that the graphitic domains in soot can occur at relatively lower temperatures[13] than charcoal[17] and that charcoal can contain a core of unburnt biomass.

Knowledge of the binding between the DNA and CMs is important for understanding the adsorption under various environmental conditions. Studies of the interaction between DNA and materials compositionally and structurally similar to soot and charcoal such as graphene, graphene oxide (GO) and reduced graphene oxide (rGO) have already provided insight into the DNA binding at CMs.[18–20] Molecular dynamics simulation suggested that, at oxygen-lacking CM's such as graphene, DNA binds to surface via the terminal base pairs through π–π stacking.[21] DNA can bind either using only one termination, with the helix axis perpendicular to the graphene surface ("standing up"), or with both terminations forming a horseshoe shape, with the axis mostly parallel to the surface except close to terminations where base pairs are severely deformed. From studies of oxygen-containing CM's such as GO and rGO, we know that DNA can bind either electrostatically via the negatively phosphate backbone (helix axis parallel to adsorbent surface - "lying down") or by π–π interaction and hydrogen bonding via the base pairs at the end of DNA,[22–24] as with graphene. In the absence of electrolytes that reduce electrostatic repulsion between negatively charged GO or rGO and negatively charged phosphate backbone, bulk adsorption studies suggest that hydrophobic forces dominate the interaction with DNA.[25] However, in the presence of electrolytes, electrostatic interaction becomes more important evidenced by increasing DNA adsorption capacity as the ionic strength increases[25,26] or as pH decreases.[25] The distribution of oxygen functional groups in GO and rGO is highly heterogeneous,[27,28] *i.e.*, they contain areas that are rich and areas that are poor in functional groups. The interaction between these surfaces and the phosphate backbone likely takes places at the areas rich in hydrophilic functional groups. In contrast, the π – π stacking takes place at areas poor in oxygen functional groups (graphene-like). Combined, these studies suggest that the ratio of hydrophilic and hydrophobic areas in carbonaceous materials determines their overall interaction with DNA, with hydrophobic interactions becoming dominant in materials rich in graphene-like surfaces.

We determined the composition of soot and charcoal using Scanning Electron Microscopy (SEM), X-ray Diffraction (XRD) and X-ray Photoelectron Spectroscopy (XPS), the structure using Raman Spectroscopy, and the surface properties using water vapour adsorption, mass titration and electrokinetic measurements. To elucidate how structure, composition and surface properties influence DNA adsorption at soot and charcoal, we measured the adsorption capacity for DNA as a function of pH, ionic strength, solution composition, time and DNA length. We propose that, besides electrostatic forces, hydrophobic interactions play an important role in adsorption of DNA to soot and charcoal. This information can be used for improving protocols of eDNA extraction from environmental matrices where soot and charcoal are abundant such as urban and wildfire aerosol,

and topsoil. This is important because DNA adsorbed at soot and charcoal could hold (paleo)biodiversity information that is not available through routine eDNA extraction and analysis. Advancing our understanding of interactions between DNA and environmental surfaces will provide an important contribution to understanding of eDNA reservoirs in the environment.

MATERIALS AND METHODS

Material characterisation

We purchased carbon soot nanopowder (NANOSHEL, >98.9%, CAS: 7440-44-0), further called soot, and activated charcoal (DARCO, Sigma Aldrich), further called charcoal. To identify major and minor contaminants, we used XRD for phase composition analysis. We placed the samples on zero-background silicon plates and collected diffractograms between 5-90 °2Θ using a Bruker D8 diffractometer equipped with Cu K_α radiation (40 kV, 40 mA; λ ~ 1.543 Å) and Baltic Instruments SolXE Si(Li) solid-state detector. We used step size of 0.04 °2Θ, time per step of 6 s and spun the sample at 20 rpm. We used 0.3° divergence and antiscatter slit and 2.3° Soller slits on both incident and diffracted beams.

We identified the trace phases using SEM. We fixed the powders on a double-sided carbon tape and sputter coated them with ~1 nm of Au. Images and energy-dispersive spectra were obtained using Vega-3 Tescan microscope equipped with 30 mm^2 Rayspec SDD detector. Both images and spectra were collected with a beam operated at 20 kV. We identified the spectral lines using IdFix software from SamX.

The surface elemental composition was determined using XPS. We used double-sided sticky tape to fix the samples. Wide and high-resolution spectra were collected using PHI X-tool instrument (Physical Electronics Inc., Chanhassen, MN, USA) (excitation energy *hv* = 1486.7 eV, tension voltage 18 kV, emission power 52 W) with a spot size of 205 μm^2. The photoelectrons were collected at 45° take-off angle using a pass energy of 280 eV with a step of 0.25 eV. The spectra calibration was done by assigning the C1s peak to 284.8 eV using PHI MultiPak 9.6.0 software.

To estimate the structural disorder of soot and charcoal, we used Raman spectroscopy. We spread the powders on Al-foil and acquired spectra with a 532 nm Ar-laser operated at 100% effect (approximately 60 mW before the objective) using a WITec alpha 300R confocal Raman microscope (WITec GmbH). The spectrometer (UHTS300 spectrometer VIS) was equipped with a back-illuminated CCD camera with Peltier cooling to -60 °C and a 600 gmm^{-1} grating, resulting in a spectral resolution of 3.8 cm^{-1}. Each spectrum was obtained as the mean of 100, 0.1 s scans. We removed signal from cosmic rays by median filtering and corrected the background by an asymmetric least square algorithm. The spectra were then Savitzky-Golay smoothened to minimise the noise. We estimated the peak areas of the smoothened spectra in the region 1200-1600 cm^{-1} using a linear baseline. At least three replicates of each sample were analysed. We used a relative intensities of G (~1560 cm^{-1}), D1 (~1350 cm^{-1}) and D2 (~1600 cm^{-1}) bands to estimate the fraction of a ordered graphitic component, *i.e.* the structural order of soot and charcoal.[29–32] In addition, we calculated *R2* parameter to estimate the disorder in soot and charcoal:[33]

$$R2 = \frac{I\ (D_1)}{I\ (D_1) + I\ (G) + I\ (D_2)}, \qquad \text{Eq 1}$$

where *I* represents an integrated area under the band.

To estimate point of zero charge (PZC), we used mass titration.[34,35] We prepared three solutions with different initial pH (pH_0 ~ 11, ~ 6 and ~ 3). 15 ml vials contained 5 ml of either 100 mM $NaNO_3$ (ACS reagent, ≥99.0%, Fluka) to estimate PZC in inert background electrolyte, and 5 and 1 mM $CaCl_2$ (dihydrate, ACS reagent, ≥99%, Roth) to estimate the effect of divalent cations on PZC. The pH was adjusted using 0.1 M HNO_3 (Fixanal, Riedel-de Haën) and 0.1 M NaOH (Fixanal, Fluka analytical) for $NaNO_3$ solution, and 0.1 M HCl (Fixanal, Fluka analytical) and 0.1 M NaOH for $CaCl_2$ solutions. We then added soot or charcoal powder to reach a target weight of a solid (wt.%), rotated the vials for ~2 h at 30 rpm for suspension to equilibrate and then measured the suspension pH before adding another batch of powder. We calculated the PZC by averaging the values of suspension pH above the solid fraction at which the pH plateaued.

For the electrokinetic measurements, we used a suspension of 1 $mgml^{-1}$ of soot and charcoal prepared with 1 and 5 mM $CaCl_2$. We titrated a 10 ml suspension with 0.05 mM HCL in 0.5 µL steps and simultaneously recorded pH and ζ potential using a Stabino instrument (Colloid Metrics GmbH, Germany).

To estimate a hydrophobic character of soot and charcoal, we volumetrically collected water vapor isotherms at 25 °C using a BELSORP-MAX instrument from BEL Japan. Prior, powders were outgassed at 150 °C for 24 h at a residual pressure of 10^{-5} – 10^{-4} Pa.

Batch adsorption experiments

Materials. We used low molecular weight salmon sperm double stranded DNA (lyophilised powder, Sigma Aldrich) with a size of ~30 base paris (bp) except for a set of experiments where we looked into the influence of DNA length on adsorption capacity of soot and charcoal where we used salmon sperm double stranded DNA solution (UltraPure, 10 $mgml^{-1}$, ThermoFischer Scientific) with the size of ≤2000 bp. We used DNA LoBind tubes (Eppendorf) and DNase/RNase-free water (molecular biology water, LONZA, AccuGene – pure water further in text) for preparation of all solutions and suspensions. The pH of stocks and suspensions was adjusted with 0.1 M HCl (EMSURE ACS reagent, 37%, Sigma Aldrich) and 0.1 M NaOH (ACS reagent, ≥97.0%, Sigma Aldrich) and measured with 913 Metrohm metre calibrated on a daily basis (precision ± 0.1 unit). We did not use pH buffers as they are known to modify DNA adsorption capacity.[36] We prepared 1 mM and 100 mM electrolyte stocks of NaCl (ACS reagent, ≥99%, anhydrous, Sigma Aldrich) and $CaCl_2$ x $6H_2O$ (ACS reagent, ≥99%, Sigma Aldrich), and soot and charcoal stock suspensions at the concentration of 50 $mgml^{-1}$. Immediately prior to an experiment, we prepared 1 $mgml^{-1}$ DNA stock (30 bp) by dissolving lyophilised powder in electrolyte suspension, shaked it for 15 min at 20 °C at 300 rpm on an orbital shaker and adjusted the pH.

Batch equilibrium adsorption. For adsorption experiments, we mixed 10 µl of a stock suspension (soot or charcoal) with the predetermined volume of electrolyte solution or pure water in 2 ml tube and ultrasonicated it for 10 min to break aggregates. We then added DNA stock to a final volume of 1 ml, vortexed the sample for a couple of seconds and placed it on a revolver rotator (18 rpm). The final mass concentration of suspensions was 0.5 – 0.6 μgml^{-1}. To obtain reliable isotherms for adsorption modelling, we prepared 5-8 different DNA concentrations between 10 – 800 μgml^{-1}, in triplicates. After 6 h of equilibration at room temperature, we centrifuged the tubes for 3 min at 5000 rpm and separated top 200 µl of the supernatant for UV spectrometry (Biophotometer, Eppendorf) using microcuvettes (BRAND). To account for turbidity, we determined the DNA concentration by subtracting the absorbance of the supernatant at 320 nm from the absorbance at 260 nm. To account for various instrumental uncertainties, the subtracted absorbance was read from a DNA calibration curve calculated on an everyday basis from freshly prepared DNA standards.

When we looked at the influence of pH, solvents (ethanol, BioReagents, absolute, Fisher Scientific; isopropanol, Bioreagent, ≥99%, Sigma Aldrich), and phosphates (Na-polyphosphate, ≥68% P_2O_5 basis, EMPLURA, Supelco; Na-metaphosphate, 96%, Sigma Aldrich) on adsorption, we followed the same protocol as for isotherms, except that the stock was diluted to only one initial DNA concentration, 50 $mgml^{-1}$.

Kinetic experiments. The kinetic experiments were done using initial DNA concentration of 50 $mgml^{-1}$, in 100 mM NaCl solution and at three temperatures: 283, 293 and 303 K (Eppendorf ThermoMixer; precision ±0.2 K). To have enough suspension to sample over the course of the experiment, we upscaled the quantities and used 15 ml instead of 2 ml tubes as was done in adsorption studies. We equilibrated the suspension and the DNA solution separately for 2 h at desired temperature before mixing them together to minimise temperature fluctuations over the course of the experiment. At various time intervals (3 min – 29 h), 200 µl of suspension were transferred to 500 µl tube and centrifuged for 3 min at 5000 rpm after which the top 150 µl was transferred to a new 500 µl tube and kept for UV measurement. The sampling time reported includes centrifugation time, i.e. the sampling time of 6 min means that the sample was equilibrated for 3 minutes in thermomixer and then centrifuged for 3 minutes.

Calculation of adsorption capacities. The equilibrium adsorption capacity of DNA (q_{eq}, μgmg^{-1}) was determined as a function of equilibrium DNA concentration in solution ($c_{eq,}$ μgml^{-1}) by taking:

$$q_{eq} = \frac{c_i - c_{eq}}{\gamma}, \qquad \text{Eq 2}$$

where c_i (μgml^{-1}) represents the initial concentration of DNA and γ represents the mass concentration of soot or charcoal ($mgml^{-1}$). For kinetic experiments, we determined the adsorption capacity q_t ($mgml^{-1}$) at time t (min):

$$q_t = c_i - c_t, \qquad \text{Eq 3}$$

where c_t (μgml^{-1}) represents DNA concentration measured in the supernatant at time t. Throughout the paper, we refer to a plot of q_{eq} vs. c_{eq} as an adsorption isotherm and to a plot of q_t vs. t as kinetic data.

Modelling of equilibrium adsorption and kinetic data. We fit the adsorption isotherms using equations that model monolayer and multilayer adsorption, and the kinetic data using equations that model surface and diffusion controlled processes (Table 1.). An overview of main assumptions and implications for each model is given in Table S1. We applied nonlinear least squares regression to fit data to models. We chose the most appropriate model by comparing their reduced chi-squared parameter of fits, χ^2_ν, *i.e.* the χ^2_ν closest to 1 was considered the best. If the best fit resulted in standard errors that were larger than the fitting parameters, the fit with χ^2_ν that was next in line but with standard errors smaller than the fitting parameters was considered more appropriate. We also report coefficients of determination, R^2, for easier comparison to studies where models were linearized and linear regression applied.

208 Table 1. Models for fitting adsorption isotherms and kinetic data.

Model		Non-linear form	Parameters	Ref.
Equilibrium adsorption				
Langmuir	Monolayer	$q_{eq} = \frac{q_{max} K_L c_{eq}}{1 + K_L c_{eq}}$	q_{max} [μgmg^{-1}] K_L [mlμg^{-1}]	37
Toth		$q_{eq} = \frac{K_T c_{eq}}{(a_T + c_{eq}^z)^{\frac{1}{z}}}$	K_T [μgmg^{-1}] a_T [μg^{z}ml^{-z}] z	38
Sips		$q_{eq} = \frac{q_{max} K_S c_{eq}^n}{1 + K_S c_{eq}^n}$	q_{max} [μgmg^{-1}] K_S [ml^{n}μg^{-n}] n	39
Freundlich	Multilayer	$q_{eq} = K_F c_{eq}^{\frac{1}{n}}$	K_F [ml$^{1/n}$μg$^{1-1/n}$mg^{-1}] n	40
Temkin		$q_{eq} = q_T \ln(A c_{eq})$	q_t [μgmg^{-1}] A [Lmg^{-1}]	41
Redlich-Peterson		$q_{eq} = \frac{K_{RP} c_{eq}}{1 + a_{RP} c_{eq}^g}$	K_{RP} [mlmg^{-1}] a_{RP} [ml^{g}μg^{-g}] 0 ≤ g ≤ 1	42
Kinetics				
Pseudo-first order (PFO)	Surface-controlled	$q_t = c_{eq}(1 - e^{-k_1 t})$	k_1 [min^{-1}] c_{eq} [μgml^{-1}]	43
Pseudo-second order (PSO)		$q_t = \frac{c_{eq}^2 k_2 t}{1 + c_{eq} k_2 t}$	k_2 [mgμg^{-1}min^{-1}] c_{eq} [μgml^{-1}]	44
Elovich		$q_t = \frac{1}{b} ln(1 + a_E b_E t)$	a_E [μgmg^{-1}min^{-1}] b_E [μgmg^{-1}] n	45
Ritchie		$q_t = q_\infty - q_\infty [1 + (n-1)\alpha t]^{\frac{1}{1-n}}$	α [min^{-1}] q_∞ [μgml^{-1}] n	46
Boyd external	Diffusion-controlled	$q_t = q_\infty (1 - e^{B_{ext} t})$	q_∞ [μgmg^{-1}] B_{ext} [min^{-1}]	47
Boyd intraparticle		$q_t = q_\infty (\frac{6}{\pi^{1.5}} \sqrt{B_{int} t} - \frac{3}{\pi^2} B_{int} t)$, $\frac{q_t}{q_\infty} < 0.85$	q_∞ [μgmg^{-1}] B_{int} [min^{-1}]	47
Weber and Morris		$q_t = k_{WM} t^{0.5}$	k_{WM} [μgmgmin$^{-0.5}$]	48

209 q_{max} – maximum adsorption capacity, K_L - Langmuir const., K_T – const., a_T – Toth const., K_F -
210 Freundlich const., R – gas const. (8.3147 JK^{-1}mol^{-1}), T – temperature (K), q_T – Temkin capacity, A –
211 Temkin isotherm const., K_{RP}, a_{RP} – Redlich-Peterson constants, K_S – Sips const., k_1 – PFO rate const.,
212 k_2 – PSO rate const., a_E – Elovich initial adsorption rate const., b_E – Elovich desorption rate const., α –
213 Ritchie nth order rate const., q_∞ - adsorption capacity at infinite time, B_{ext} – Boyd external rate

coefficient, B_{int} – Boyd intraparticle rate coefficient, k_{WM} – Webber and Morris intraparticle diffusion coefficient, *z, n, g* – power constants.

RESULTS AND DISCUSSION

Composition and properties of soot and charcoal

Phase and elemental composition. Both soot and charcoal are largely composed of poorly ordered graphite-like carbon material as evidenced by the presence of broad diffraction peaks between 15 - 30 °2Θ, corresponding to graphite (001) reflection, and 40 - 50 °2Θ, corresponding to a combination of graphite (100) and (101) reflections (Fig. 1A). In addition, soot contains quartz (SiO_2) as a minor impurity identified by XRD and trace amounts of titanite ($CaTiSiO_5$; Fig. S1a) and chlorapatite ($Ca_5(PO_4)_3Cl$; Fig. S1b) identified by EDX spectroscopy. Charcoal contains minor quartz and Na-rich plagioclase ($(Na,Ca)(Al,Si)_4O_8$) (Fig. 1A), and trace amounts of likely a Ca-Mg carbonate (either Mg-calcite ($CaCO_3$) or dolomite ($CaMg(CO_3)_2$; Fig. S2b), an Fe-O phase (Fig. S2c) and TiO_2 phase (Fig. S2d). XPS showed that the surface of soot contained 90.9 At.% of C and 9.1 At.% of O with trace amount of Si, N and S while charcoal contained 93.0 At.% of C and 7.0 At.% of O with trace amount of N, Si and Al (Figure 1B). Since quartz and plagioclase contain Si and Al, the small surface concentration of these elements confirm that the contribution of mineral impurities to reactions at soot and charcoal surfaces is likely negligible.

Structural (Raman) properties. We observed three bands in Raman spectra of soot and charcoal (Fig. 1C-D): D_1 (~1350 cm^{-1}), G (~1560 cm^{-1}) and D_2 (~1600 cm^{-1}) bands. The Raman shift of the bands is comparable between soot (D_1= 1348 ± 6 cm^{-1}, G= 1567 ± 2 cm^{-1}, D_2= 1598 ± 2 cm^{-1}) (Fig. 1C) and charcoal (D_1= 1348 ± 5 cm^{-1}, G= 1563 ± 2 cm^{-1}, D_2= 1606 ± 2 cm^{-1}) (Fig. 1D). For soot the G band is relatively more intense compared to both D_1 and D_2 than for charcoal suggesting that soot contains larger volume of an ordered graphitic component. *R2* parameter (Eq. 1) is smaller for soot (0.554 ± 0.027) compared to charcoal (0.642 ± 0.006) indicating that soot is overall more ordered and more graphite-like than charcoal.

Surface properties. In an inert electrolyte (100 mM $NaNO_3$), the PZC of soot (8.3 ± 0.1; Fig. S3a) and charcoal (9.5 ± 0.1; Fig. S3b) was comparable to previous studies on CMs that used mass titration.[49–52] In $CaCl_2$ solutions, the PZC was lower than in $NaNO_3$ for both soot (7.7 ± 0.1; Fig. 1E) and charcoal (8.3 ± 0.2; Fig. 1F) likely reflecting an increase in surface charge density in divalent electrolyte solutions. The IEP for both materials determined by electrokinetic measurements, however, was significantly lower: for soot, IEP in 1 mM $CaCl_2$ was ~ 3.4 and in 5 mM CaCl2 ~ 3.6 (Fig. 1G) while for charcoal it was ~ 3.0 in 1 mM $CaCl_2$ and 3.0 – 3.5 in 5 mM $CaCl_2$ (Fig. 1H). The increase of IEP with an increase in ionic strength reflects a more efficient screening of negatively charged active sites. A higher PZC than IEP indicates a heterogeneous distribution of surface charges where external particle surfaces are more negatively charged than internal surfaces,[51] suggesting that both soot and charcoal behave as negatively charged surfaces in circumneutral solutions.

Both soot and charcoal adsorbed only 2 - 3 molecules of water at low pressures (p/p_0<0.4, Fig. 1I), a characteristic of hydrophobic surfaces.[53,54] The difference in the adsorbed water between soot and charcoal is <0.1 molecule/nm, reflecting a similar surface composition determined with XPS (Fig. 1B) and suggesting no significant difference in bulk hydrophobicity between soot and charcoal.

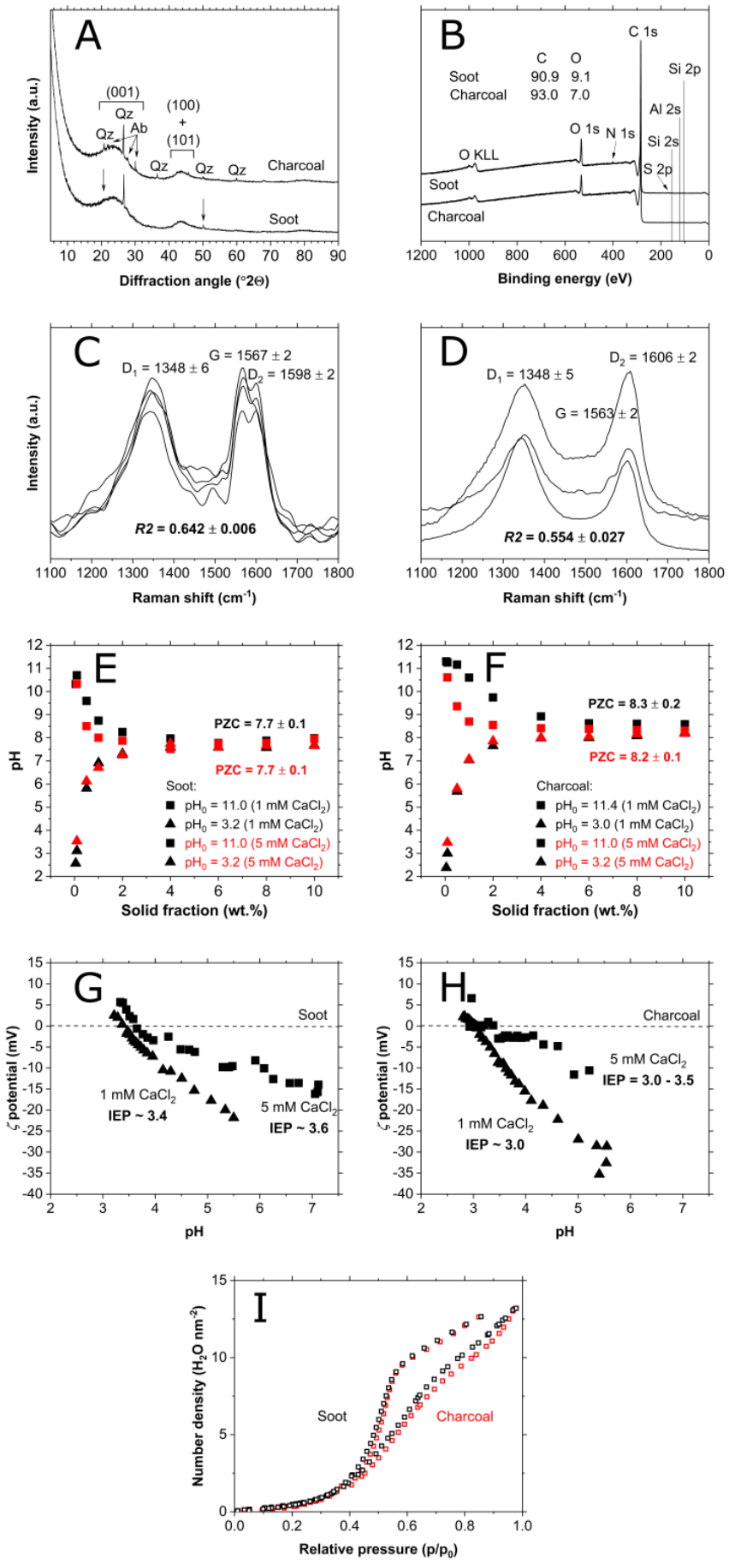
A
Intensity (a.u.)
(001)
Qz
Qz
Ab
(100)
+
(101)
Qz
Qz
Qz
Charcoal
Soot
Diffraction angle (°2Θ)
B
C 1s
C O
Soot 90.9 9.1
Charcoal 93.0 7.0
Si 2p
Al 2s
O 1s
N 1s
Si 2s
O KLL
S 2p
Soot
Charcoal
Binding energy (eV)
C
D1 = 1348 ± 6
G = 1567 ± 2
D2 = 1598 ± 2
R2 = 0.642 ± 0.006
Intensity (a.u.)
Raman shift (cm-1)
D
D1 = 1348 ± 5
D2 = 1606 ± 2
G = 1563 ± 2
R2 = 0.554 ± 0.027
Raman shift (cm-1)
E
PZC = 7.7 ± 0.1
PZC = 7.7 ± 0.1
Soot:
pH0 = 11.0 (1 mM CaCl2)
pH0 = 3.2 (1 mM CaCl2)
pH0 = 11.0 (5 mM CaCl2)
pH0 = 3.2 (5 mM CaCl2)
pH
Solid fraction (wt.%)
F
PZC = 8.3 ± 0.2
PZC = 8.2 ± 0.1
Charcoal:
pH0 = 11.4 (1 mM CaCl2)
pH0 = 3.0 (1 mM CaCl2)
pH0 = 11.0 (5 mM CaCl2)
pH0 = 3.2 (5 mM CaCl2)
pH
Solid fraction (wt.%)
G
Soot
1 mM CaCl2
IEP ~ 3.4
5 mM CaCl2
IEP ~ 3.6
ζ potential (mV)
pH
H
Charcoal
5 mM CaCl2
IEP = 3.0 - 3.5
1 mM CaCl2
IEP ~ 3.0
ζ potential (mV)
pH
I
Soot
Charcoal
Number density (H2O nm-2)
Relative pressure (p/p0)

255

Figure 1. a) XRD patterns with assigned diffraction peaks from the graphite structure; Qz – quartz and Ab- albite occur as minor components. b) XPS results and quantitative analysis with assigned photoelectron peaks. c) soot and d) charcoal Raman spectra containing peak assignment and their shift. Uncertainties are reported as a range of detected shifts. Mass titration with e) soot and f) charcoal started from different initial pH values (pH_0). Electrokinetic measurements of g) soot and h) charcoal with the corresponding isoelectric points (IEP) determined as an average between neighbouring data points above and below 0 mV. h) Number of H_2O molecules per surface area is similar between soot (black) and charcoal (red) as determined from water adsorption measurements.

Adsorption

pH dependence. The equilibrium adsorption capacity (q_{eq}) of DNA at soot and charcoal decreases as pH increases (Figure 2A). The capacity is lowest between 6 < pH < 8 (soot = 61 ± 1 μgmg^{-1}, charcoal = 72 ± 0 μgmg^{-1}). At pH<6, the capacity increases reaching the maximum at pH=3 (soot = 70 ± 2 μgmg^{-1}, charcoal = 83 ± 2 μgmg^{-1}). Since the pK_a of the phosphoester in the backbone of DNA is ~1, and soot and charcoal behave as negatively charged particles above ~3 (Fig. 1G-H), a decrease in adsorption capacity with an increase in pH suggests that the electrostatic interaction plays a role in the interaction. One would expect that at circumneutral pH, when both DNA, and soot and charcoal are negatively charged, the adsorption would be minimal and the capacity would be close to zero. However, a significant amount of DNA is still adsorbed: at both soot and charcoal there is still ~86% of DNA of the capacity at pH = 3. This cannot be due to adsorption at inner particle surfaces that are more positive than the outer (Figure 1E-F) because the outer surfaces are even more negative at circumneutral pH (< -10 mV, Fig. 1G-hH) thus repelling DNA. This suggest that the electrostatics is not the only interaction governing the adsorption.

Adsorption isotherms. In all solutions and at all DNA concentrations, the adsorption capacity of charcoal was higher than that of soot (Figure 2B-C). This is even more pronounced when comparing the adsorption capacity per surface area since specific surface area of charcoal is smaller (923 m^2g^{-1}) than of soot (973 m^2g^{-1}) (Table S2). As the equilibrium solution concentration of DNA (c_{eq}) increased, q_{eq} of both soot (Figure 2B) and charcoal (Figure 2C) increased abruptly until c_{eq} ~ 100 μgmg^{-1} after which the increase is gradual. Regardless of the cation, q_{eq} was always higher at high cation concentration (100 mM – full symbols) than at low (1 mM – empty simbols), likely because of more efficient screening of electrostatic repulsion between negatively charged DNA, and soot and charcoal surfaces. The influence of cation valency is not as straightforward. For charcoal, larger q_{eq} in $CaCl_2$ than in NaCl solution was consistently observed in the whole range of c_{eq}'s. For soot, however, the q_{eq} was highest in $CaCl_2$ solution below c_{eq} ~ 400 μgml^{-1} but above c_{eq} ~ 450 μgml^{-1}, q_{eq} was comparable or even lower in $CaCl_2$ than in NaCl solution. DNA adsorbed at soot and charcoal even in pure water although with the lowest q_{eq} measured. The occurrence of adsorption in pure water, *i.e.* in absence of charge screening cations again suggest that electrostatic interaction is not the only one governing the adsorption.

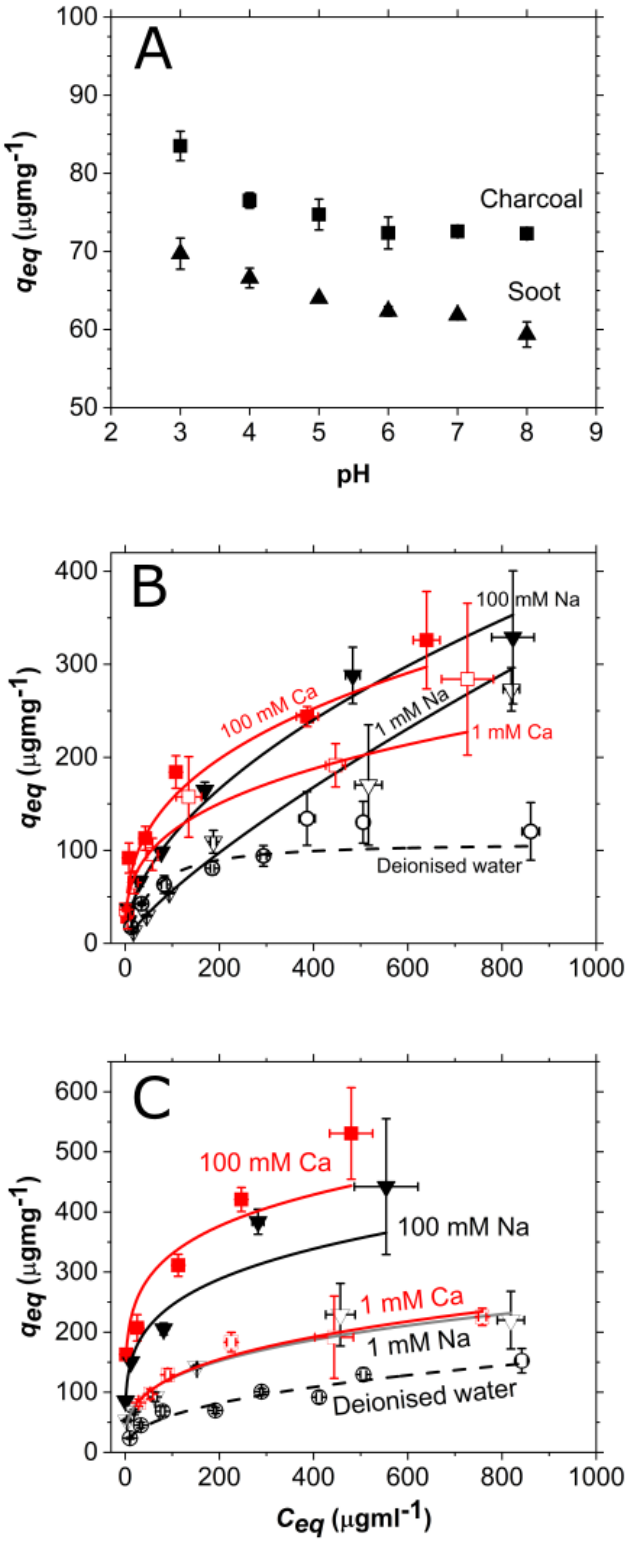

Figure 2. a) DNA adsorption capacity decreases as pH increases in solution with 100 mM NaCl and with initial DNA concentration of 50 µgml^{-1}. Adsorption isotherms for b) soot and c) charcoal. Experimental data are represented with symbols and best fits with lines (Freundlich model except for soot in 1 mM $CaCl_2$ solution and deionised water that was best fit with the Sips model). All uncertainties given as standard deviation.

To quantitatively describe the measured sorption relationships, we fit a range of models (Table 1) to the adsorption isotherms (Figure 2B-C, full lines). Based on χ^2_v and R^2 parameters, the best fit was to the Freundlich model, except for DNA adsorption at soot in pure water and 1 mM $CaCl_2$: in these cases, the data was best described with the Sips model (Tables 2 and S3). The fit to the Freundlich model suggests that the DNA adsorption is a multilayer process[40] and that the surfaces are energetically heterogeneous, *i.e.* the surface sites at which the adsorption occurs are not of the same energy and abundance. At charcoal, the Freundlich constant, K_F, and the exponent, n, are lowest for adsorption in pure water (Table 2) suggesting that both the adsorption affinity towards DNA (estimated with K_F)[55] and the heterogeneity of the surface (estimated with n)[55] are lowest when there are no cations in solution. The dependence between K_F and n, and cation concentration and valency is expected since both the surface heterogeneity of a material and the surface charge density vary as a function of ionic strength, which influences the surface potential.[56] The surface affinity towards DNA and the charcoal surface heterogeneity in the presence of 1 mM is significantly lower than in the presence of 100 mM of either Na^+ or Ca^{2+}. Thus, the DNA adsorption capacity at charcoal follows the trend (Table 2):

$$q_{eq}\text{ (DNA, charcoal)} \rightarrow \text{pure water} < 1\text{ mM NaCl} \sim 1\text{ mM } CaCl_2 < 100\text{ mM NaCl} < 100\text{ mM } CaCl_2. \quad \text{Eq 4}$$

We observed a similar trend for adsorption at soot that was best described with the Freundlich model (Table 2):

$$q_{eq}\text{ (DNA, soot)} \rightarrow 1\text{ mM NaCl} < 100\text{ mM NaCl} < 100\text{ mM } CaCl_2. \quad \text{Eq 5}$$

In contrast, the better fit of isotherms at soot in pure water and 1 mM $CaCl_2$ to the Sips model suggests that the surface is still best described as energetically heterogeneous although DNA adsorbs as monolayer,[39] *i.e.* there exists a maximum adsorption capacity (q_{max}) (Table 2). q_{max}, and in fact q_{eq} at each c_{eq}, at soot in 1 mM $CaCl_2$ solution is ~3.5x higher than in pure water, *i.e.*:

$$q_{eq}\text{ (DNA, soot)} \rightarrow \text{pure water} < 1\text{ mM } CaCl_2. \quad \text{Eq 6}$$

Table 2. Fitted parameters for Freundlich and Sips isotherm models for adsorption of DNA at soot and charcoal in pure water, 100 mM and 1 mM NaCl (Na) and $CaCl_2$ (Ca) solutions.

		Freundlich			
		K_F	n	χ^2_v	
Charcoal	Water	9.33 ± 1.23	2.44 ± 0.16	2.39	
	1 Na	31.46 ± 3.98	3.36 ± 0.31	3.21	
	100 Na	72.08 ± 6.02	3.58 ± 0.39	7.04	
	1 Ca	29.70 ± 3.73	3.21 ± 0.26	0.89	
	100 Ca	139.42 ± 5.66	5.33 ± 0.49	3.54	
Soot	1 Na	1.53 ± 0.20	1.26 ± 0.05	1.08	
	100 Na	9.83 ± 1.98	1.87 ± 0.16	1.65	
	100 Ca	31.27 ± 8.90	2.87 ±0.43	2.35	
			Sips		
		K_s	Q_{max}	n_s	χ^2_v
	Water	0.010 ± 0.001	108 ± 11	1.16 ± 0.11	1.03
	1 Ca	0.079 ± 0.066	350 ± 298	0.42 ± 0.13	1.02

A ramification of the Sips equation is that when n_s = 1, the model reduces to the Langmuir equation (Table 1) indicating that the surface is homogeneous, *i.e.* there is only one type of adsorption site. The n_s = 1.16 for adsorption at soot in pure water suggesting that DNA adsorbs at few active sites which eventually become saturated. This is also corroborated with good fits of the isotherm obtained in pure water to the Langmuir model (Table S3; χ^2_v =1.24, R^2 = 0.9789). However, n_s = 0.42 for adsorption in 1 mM $CaCl_2$, suggesting that the surface is heterogeneous with many active adsorption sites. Therefore, we conclude that, for soot, the surface heterogeneity in electrolyte solutions is a consequence of strong ion binding and formation of new sites. In contrast to soot, charcoal contains many active sites for DNA adsorption already in pure water and gains more with strong ion binding as solution concentration increases (as described with the fit to Freundlich model).

Adsorption kinetics. To obtain a more comprehensive insight into the mechanism of DNA adsorption at charcoal and soot, we studied how the concentration of adsorbed DNA, q_t, varies as a function of time, t, at three different temperatures, 283 K, 293 K and 303 K (Figure 3A-B). q_t started plateauing at ~300 min suggesting that the equilibrium was reached. We continued to monitor the q_t for another 24 h to obtain a reliable estimates of q_t at infinite time, q_∞.

Adsorption of DNA at soot and charcoal happens quickly. For soot, 50% of the DNA adsorbed after 29 h (1740 min) was already adsorbed in <1 min at 303 K, ~1 min at 293 K and ~3 min at 283 K (Figure 3A). For charcoal, the adsorption of 50% of DNA was slightly slower- ~1 min at 303 K, ~2 min at 293 K and ~4 min at 283 K (Figure 3B). After 360 min, both soot and charcoal adsorbed ~98% of the DNA adsorbed after 29 h at all temperatures.

To quantitatively assess these observations, we fit the kinetic data to various adsorption kinetic models (Table 1). The best fit was achieved with the Ritchie 3rd order kinetic model (Table S4). This, however, suggests that the adsorption is not diffusion-controlled but surface-controlled, *i.e.* the mass transfer depends only on the rate of DNA adsorption on active surface sites and not the rate of its transfer through the bulk solution to the particle or through particle pores. Based on the assumptions of the Ritchie model,[46] we deduce that the adsorption is dominated by the interaction with adsorption sites and not by the lateral interactions between neighbouring molecules and that each DNA molecule occupies three active sites (n = 3).

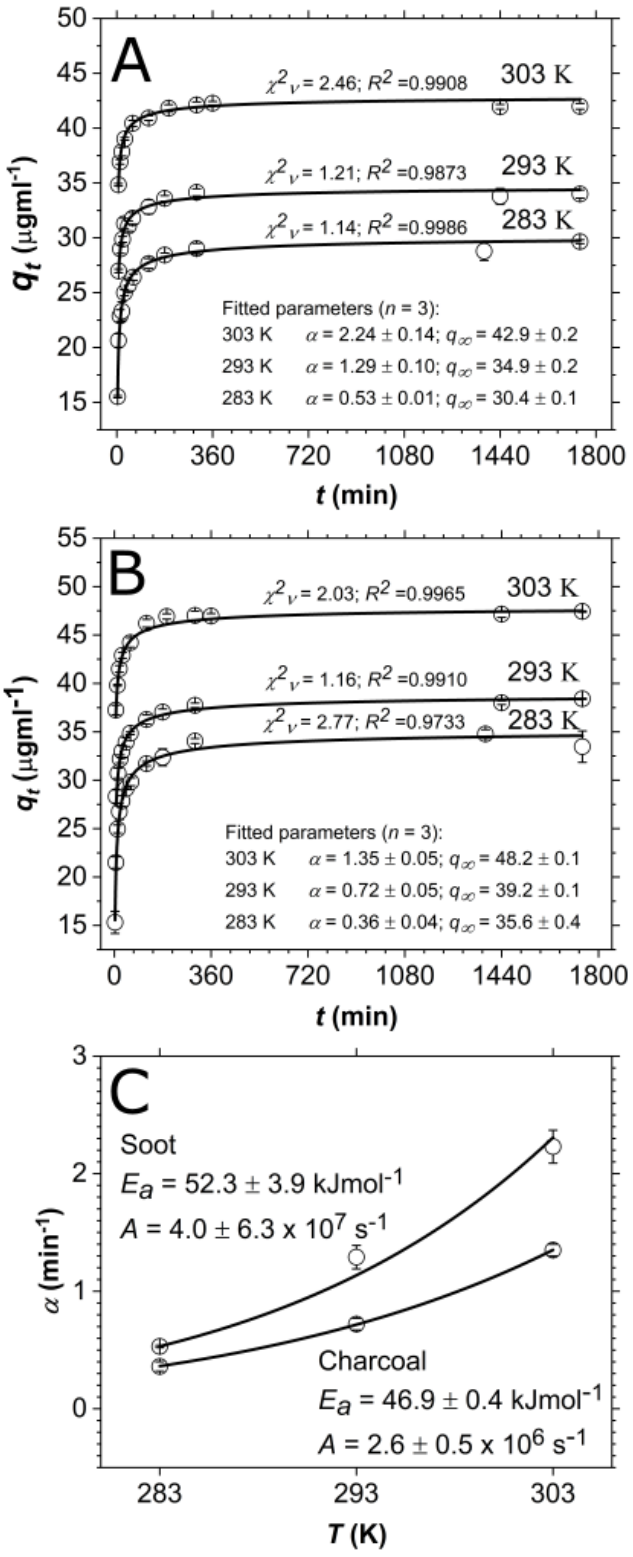

Figure 3. Kinetic experimental data (empty circle) with the Ritchie kinetic model (full line), corresponding quality of fits (χ^2_ν, R^2) and fitted parameters for a) soot and b) charcoal. q_∞ expressed in μgml^{-1} and α in min^{-1}. Adsorption conducted in 100 mM NaCl and pH = 7. c) Arrhenius plot derived from the kinetic rates (empty circle) showing a logarithmic fit to the data (full line) with the calculated adsorption activation energy (E_a) and the kinetic pre-factor (A). All uncertainties given as standard deviation.

To estimate the activation energy, E_a, required for adsorption of DNA at soot and charcoal, we plotted α as a function of temperature, T (Figure 3C). We calculated E_a by fitting the plot to the Arrhenius equation:[57]

$$\alpha = Ae^{\frac{E_a}{RT}}, \qquad \text{Eq 7}$$

where A represents kinetic pre-factor (min^{-1}), and R the gas constant (8.3145 J $mol^{-1}K^{-1}$). We observed that somewhat higher energy is required to adsorb DNA at soot (E_a = 52.3 ± 3.9 $kJmol^{-1}$) than at charcoal (E_a = 46.9 ± 0.4 $kJmol^{-1}$) suggesting that interaction between DNA and soot is stronger than DNA and charcoal. Given the heterogeneous nature of the active sites at soot and charcoal, the E_a's calculated using the Arrhenius equation are an average of likely many E_a's governing DNA adsorption. Regardless, the E_a's are >40 $kJmol^{-1}$, a rule of thumb value for differentiation between a physisorption and chemisorption, indicating a strong, perhaps a covalent interaction between DNA, and soot and charcoal.

Adsorption of long DNA. For soils, the length of DNA influences the q_{eq}[58,59] and likely the overall adsorption mechanism. To explore the role of DNA length on adsorption to CMs, we collected adsorption isotherms using <2000 kb DNA (long DNA) in 100 mM NaCl and in pure water (Figure 4). Similarly to q_{eq} for ~30 kb DNA (short DNA) (Figure 2B-C), q_{eq} for long DNA at charcoal is larger than at soot in 100 mM NaCl. However, this is not the case in pure water where q_{eq} is higher at soot than at charcoal. This is the only instance where adsorption at soot was higher than at charcoal (Fig. 2B-C, Table 2). These observations can be explained by enhanced hydrophobic interactions in pure water compared to electrolytes where charges give rise to electrostatic attractive interaction.

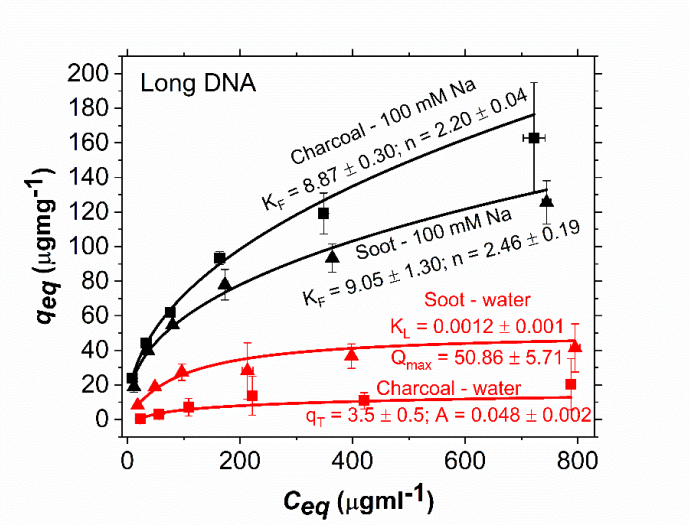

Figure 4. Adsorption experimental data (symbols) of <2000 bp salmon sperm DNA and the corresponding isotherm models (lines). Table S5 contains quality of fit parameters. The capacity for long DNA is lower than for short DNA (Figure 2). There is a significantly larger difference in the adsorption capacity of DNA in pure water and 100 mM NaCl at charcoal than at soot. This suggest that different interaction forces control adsorption of DNA at those two materials, likely reflecting a difference in the magnitude of the hydrophobic interaction. All uncertainties given as standard deviation. K_F = Freundlich constant, K_L = Langmuir constant, Q_{max} = maximum adsorption capacity, q_T = Temkin capacity, A = Temkin isotherm constant (units in Table 1).

The fitting to isotherm models revealed very similar behaviour as for the short DNA: The adsorption of long DNA in electrolytes is best explained by a multilayer adsorption process that happens at

energetically heterogeneous surface (quality of fit parameters in Table S5, model fits in Figure 4). A better fit of the isotherm for charcoal in pure water to Temkin rather than Freundlich model suggest that there is either a uniform distribution of heterogeneous binding sites or that there is interaction between neighbouring DNA molecules.[60] Long DNA adsorption at soot in pure water is still best explained by a monolayer adsorption but the adsorption sites are energetically similar (Langmuir model). This stands in contrast to monolayer adsorption of short DNA at heterogeneous surface (Sips model, Table 2).

In contrast to fits to the experimental data of short DNA where one single model had unquestionably better quality of fit parameters (Table S3), for long DNA many of the tested models often fit the data well. Some fits had χ^2_ν very close to 1 but the value of standard deviation was larger than the fitted model parameters (red in Table S5). In these cases, we considered as the best that fit that had χ^2_ν next in line but had standard deviation smaller than the fitted model parameters. These fits often had larger R^2 compared to the fit with χ^2_ν closest to 1. The fact that the fitting parameters do not give a conclusive picture about the adsorption of long DNA suggests that the mechanism is likely more complicated than in the case of short DNA. However, we did observe that all models that closely fit experimental data had similar assumptions and implications, *i.e.* adsorption of long DNA at soot in pure water is similarly well fit with both Langmuir and Toth models (Table S5). Since the *z* parameter of Toth model was ~1, this suggests that the adsorption is in fact a monolayer process but there might be more than one active site as by the good fit to the Langmuir model.

Long DNA showed lower q_{eq} than short DNA both in 100 mM NaCl and pure water. This is a result of either enhanced steric hindrances as a consequence of size and charge variations of DNA or diffusion limited mass transfer of long DNA.[58,61] If steric hindrances increase with size, that would suggest that the phosphate backbone of DNA is responsible for interaction with soot and charcoal surfaces. To test this, we adsorbed short DNA in presence of polyphosphate and metaphosphate (Figure 5) that compete with DNA for adsorption sites at negatively charged surfaces such as clay minerals.[59,62] We did not observe any changes in q_{eq} of DNA for a wide range of phosphate concentrations

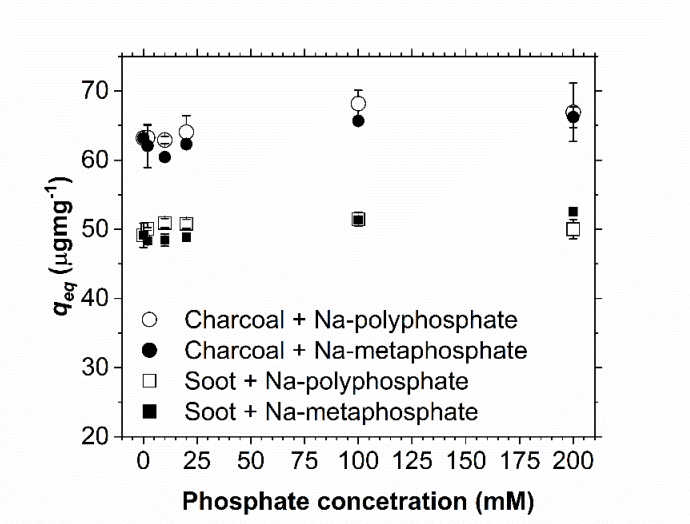

Figure 5. q_{eq} does not significantly vary as a function of concentration of Na-polyphosphate and Na-metaphosphate suggesting that phosphate backbone of DNA does not play a significant role in adsorption to soot and charcoal. Initial DNA concentration was ~50 μgml^{-1} and we used a solution of 100 mM NaCl. Uncertainties expressed as standard deviation.

(0-200 mM PO_4^{3-} equivalent) suggesting that phosphate backbone is not responsible for DNA interaction with soot and charcoal, fitting well with the experiments conducted using graphene materials.[25] Since the steric repulsion cannot account for lower capacity of long compared to short DNA, the alternative explanation by which the adsorption is diffusion limited implies that a different mechanism controls adsorption of long and short DNA.

Hydrophobic interactions. To test our hypothesis that the hydrophobic forces play an important role in DNA adsorption at soot and charcoal, we measured the q_{eq} in mixtures of pure water and ethanol, and pure water and isopropanol (Figure 6). These alcohols have lower dielectric constant than water (ε(water) = 80, ε(ethanol) = 25, ε(isopropanol) = 18) so mixing them decreases the interfacial tension of water in contact with a hydrophobic surface, effectively decreasing the hydrophobic interactions.[63,64] If hydrophobic interactions influence adsorption, water-alcohol mixtures ought to retain DNA in solution because the entropic drive for partitioning DNA from the solution to the hydrophobic surface is diminished. We observed exactly that, a decrease in DNA adsorption with increasing volume fraction of either ethanol or isopropanol in the solution (Fig. 6A-B). In addition, a q_{eq} in isopropanol was consistently lower than in ethanol solution, as expected since isopropanol is less polar than ethanol so there is a lower drive for DNA to escape it. An exception to this is a larger q_{eq} at 60 vol.% where we likely already observed DNA precipitation in isopropanol but not in ethanol since higher ionic strengths are needed for DNA precipitation in ethanol mixtures.[65] Such adsorption behaviour was also observed on graphene oxide,[25] which is significantly more hydrophilic than either soot or charcoal.

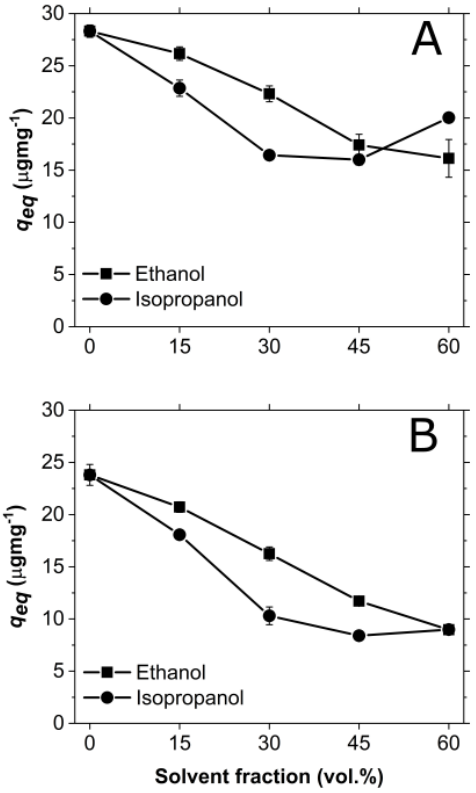

Figure 6. Equilibrium adsorption capacity of DNA at a) soot and b) charcoal decreases as the alcohol concentration in the solution increases suggesting hydrophobic interaction plays a role in the DNA sorption to both materials. Initial DNA concentration was 50 μgml^{-1}. Full lines are not the fit, and only serve as a guide to the eye.

Since the bulk hydrophobicity of both CM's is similar, the higher q_{eq} at soot than charcoal in pure water is perhaps a consequence of a strong heterogeneous distribution of hydrophobic sites at soot. This heterogeneity at soot is likely reflected in a more complex modeling of DNA adsorption (eqs 5 and 6) compared to charcoal (eq 4).

Elucidating the role of CMs in adsorption and stabilization of eDNA is important for better understanding of its cycling in environment. This study revealed that the adsorption capacity of DNA at soot and charcoal increases as pH decreases and as ionic strength increases, and it is generally higher for solutions containing divalent compared to monovalent cations. The majority of DNA adsorbs within minutes at both CMs with the activation energy of ~50 $kJmol^{-1}$ suggesting a strong, perhaps covalent binding. Our results imply that DNA binds to both CM's by terminal basepairs and we showed that both electrostatic and hydrophobic interactions are important contributors to adsorption. The contribution of one or another interaction depends likely on the relative proportion of graphitic (hydrophobic) surfaces and those populated by oxygen functional groups. Combined, this study provides a fundamental understanding of DNA-CM interactions that can be used for improving DNA extraction protocols from environmental matrices containing CM. Our results demonstrate that CM's are likely reservoirs of extracellular eDNA in urban aerosol and topsoil and environments under influence of wildfires. These reservoirs can potentially be used for monitoring of biodiversity, and invasive and endangered species.

ACKNOWLEDGMENTS

We thank Enrico Cappellini for access to Biophotometer. KKS and SJ are grateful for a research grant from VILLUM FONDEN (00025352). SJ was partly funded by French Government through MOPGA Postdoctoral Programme (reference number 3—5402234721). The geochemistry-mineralogy platform of ISTerre (Grenoble, France) is partially funded by a grant from Labex OSUG@2020 (investissements d'avenir, ANR10-LABX56). SM was funded by the VILLUM FONDEN (Grant numbers 00022942).

CONFLICTS OF INTEREST

Authors declare no conflicts of interest.

REFERENCES:

1. Slon, V. *et al.* Neandertal and Denisovan DNA from Pleistocene sediments. *Science* **356**, 605–608 (2017).
2. Pedersen, M. W. *et al.* Environmental genomics of Late Pleistocene black bears and giant short-faced bears. *Current Biology* **31**, 2728-2736.e8 (2021).
3. Romanowski, G., Lorenz, M. G. & Wackernagel, W. Adsorption of plasmid DNA to mineral surfaces and protection against DNase I. *Appl. Environ. Microbiol.* **57**, 1057–1061 (1991).
4. Paget, E., Monrozier, L. J. & Simonet, P. Adsorption of DNA on clay minerals: protection against DNaseI and influence on gene transfer. *FEMS Microbiology Letters* **97**, 31–39 (1992).
5. Khanna, M. & Stotzky, G. Transformation of Bacillus subtilis by DNA bound on montmorillonite and effect of DNase on the transforming ability of bound DNA. *Appl Environ Microbiol* **58**, 1930–1939 (1992).

6. Thomsen, P. F. & Willerslev, E. Environmental DNA – An emerging tool in conservation for monitoring past and present biodiversity. *Biological Conservation* **183**, 4–18 (2015).
7. Bohmann, K. *et al.* Environmental DNA for wildlife biology and biodiversity monitoring. *Trends in Ecology & Evolution* **29**, 358–367 (2014).
8. Pedersen, M. W. *et al.* Ancient and modern environmental DNA. *Philosophical Transactions of the Royal Society B: Biological Sciences* **370**, 20130383 (2015).
9. Taberlet, P., Bonin, A., Zinger, L. & Coissac, E. *Environmental DNA: For Biodiversity Research and Monitoring*. (Oxford University Press, 2018). doi:10.1093/oso/9780198767220.001.0001.
10. Clare, E. L. *et al.* Measuring biodiversity from DNA in the air. *Current Biology* **32**, 693-700.e5 (2022).
11. Lynggaard, C. *et al.* Airborne environmental DNA for terrestrial vertebrate community monitoring. *Current Biology* **32**, 701-707.e5 (2022).
12. Schmidt, M. W. I. & Noack, A. G. Black carbon in soils and sediments: Analysis, distribution, implications, and current challenges. *Global Biogeochemical Cycles* **14**, 777–793 (2000).
13. Xi, J., Yang, G., Cai, J. & Gu, Z. A Review of Recent Research Results on Soot: The Formation of a Kind of Carbon-Based Material in Flames. *Frontiers in Materials* **8**, 179 (2021).
14. Franklin, R. E. & Randall, J. T. Crystallite growth in graphitizing and non-graphitizing carbons. *Proceedings of the Royal Society of London. Series A. Mathematical and Physical Sciences* **209**, 196–218 (1951).
15. Sadezky, A., Muckenhuber, H., Grothe, H., Niessner, R. & Pöschl, U. Raman microspectroscopy of soot and related carbonaceous materials: Spectral analysis and structural information. *Carbon* **43**, 1731–1742 (2005).
16. Müller, J.-O., Su, D. S., Wild, U. & Schlögl, R. Bulk and surface structural investigations of diesel engine soot and carbon black. *Phys. Chem. Chem. Phys.* **9**, 4018–4025 (2007).
17. Pyle, L. A. *et al.* Chemical and Isotopic Thresholds in Charring: Implications for the Interpretation of Charcoal Mass and Isotopic Data. *Environ. Sci. Technol.* **49**, 14057–14064 (2015).
18. Szabó, T. *et al.* Evolution of Surface Functional Groups in a Series of Progressively Oxidized Graphite Oxides. *Chem. Mater.* **18**, 2740–2749 (2006).
19. Knauer, M. *et al.* Soot Structure and Reactivity Analysis by Raman Microspectroscopy, Temperature-Programmed Oxidation, and High-Resolution Transmission Electron Microscopy. *J. Phys. Chem. A* **113**, 13871–13880 (2009).
20. Erickson, K. *et al.* Determination of the Local Chemical Structure of Graphene Oxide and Reduced Graphene Oxide. *Advanced Materials* **22**, 4467–4472 (2010).
21. Zhao, X. Self-Assembly of DNA Segments on Graphene and Carbon Nanotube Arrays in Aqueous Solution: A Molecular Simulation Study. *J. Phys. Chem. C* **115**, 6181–6189 (2011).
22. He, S. *et al.* A Graphene Nanoprobe for Rapid, Sensitive, and Multicolor Fluorescent DNA Analysis. *Advanced Functional Materials* **20**, 453–459 (2010).
23. Lei, H. *et al.* Adsorption of double-stranded DNA to graphene oxide preventing enzymatic digestion. *Nanoscale* **3**, 3888–3892 (2011).

24. Tang, L., Chang, H., Liu, Y. & Li, J. Duplex DNA/Graphene Oxide Biointerface: From Fundamental Understanding to Specific Enzymatic Effects. *Advanced Functional Materials* **22**, 3083–3088 (2012).

25. Wu, M., Kempaiah, R., Huang, P.-J. J., Maheshwari, V. & Liu, J. Adsorption and Desorption of DNA on Graphene Oxide Studied by Fluorescently Labeled Oligonucleotides. *Langmuir* **27**, 2731–2738 (2011).

26. Huang, P.-J. J. & Liu, J. Molecular Beacon Lighting up on Graphene Oxide. *Anal. Chem.* **84**, 4192–4198 (2012).

27. Liu, Z. *et al.* Direct observation of oxygen configuration on individual graphene oxide sheets. *Carbon* **127**, 141–148 (2018).

28. Liu, Z., Rios-Carvajal, T., Ceccato, M. & Hassenkam, T. Nanoscale chemical mapping of oxygen functional groups on graphene oxide using atomic force microscopy-coupled infrared spectroscopy. *Journal of Colloid and Interface Science* **556**, 458–465 (2019).

29. Tuinstra, F. & Koenig, J. L. Raman Spectrum of Graphite. *J. Chem. Phys.* **53**, 1126–1130 (1970).

30. Beny-Bassez, C. & Rouzaud, J. N. Characterization of Carbonaceous Materials by Correlated Electron and Optical Microscopy and Raman Microspectroscopy. *Scanning Electron Microscopy* 119–132 (1985).

31. Wang, Y., Alsmeyer, D. C. & McCreery, R. L. Raman spectroscopy of carbon materials: structural basis of observed spectra. *Chem. Mater.* **2**, 557–563 (1990).

32. Sze, S.-K., Siddique, N., Sloan, J. J. & Escribano, R. Raman spectroscopic characterization of carbonaceous aerosols. *Atmospheric Environment* **35**, 561–568 (2001).

33. Beyssac, O., Goffé, B., Chopin, C. & Rouzaud, J. N. Raman spectra of carbonaceous material in metasediments: A new geothermometer. *Journal of Metamorphic Geology* **20**, 859–871 (2002).

34. Ŝalac, S. & Kallay, N. Application of mass titration to the point of zero charge determination. *Journal of Colloid and Interface Science* **149**, 233–240 (1992).

35. Preočanin, T. & Kallay, N. Application of »Mass Titration« to Determination of Surface Charge of Metal Oxides. *Croatica Chemica Acta* **71**, 1117–1125 (1998).

36. Saeki, K., Kunito, T. & Sakai, M. Effect of Tris-HCl Buffer on DNA Adsorption by a Variety of Soil Constituents. *Microbes and Environments* **26**, 88–91 (2011).

37. Langmuir, I. THE ADSORPTION OF GASES ON PLANE SURFACES OF GLASS, MICA AND PLATINUM. *J. Am. Chem. Soc.* **40**, 1361–1403 (1918).

38. Rudzinski, W. & Everett, D. *Adsorption of Gases on Heterogeneous Surfaces*. (Academic Press, 1991).

39. Sips, R. On the Structure of a Catalyst Surface. *J. Chem. Phys.* **16**, 490–495 (1948).

40. Freundlich, H. Über die Adsorption in Lösungen. *Zeitschrift für Physikalische Chemie* **57U**, 385–470 (1907).

41. Temkin, M. I. The Kinetics of Some Industrial Heterogeneous Catalytic Reactions. in *Advances in Catalysis* (eds. Eley, D. D., Pines, H. & Weez, P. B.) vol. 28 173–291 (Academic Press, 1979).

42. Redlich, O. & Peterson, D. L. A Useful Adsorption Isotherm. *J. Phys. Chem.* **63**, 1024–1024 (1959).

43. Lagergren, S. Zur theorie der sogenannten adsorption gelöster stoffe. *Kungliga Svenska Vetenskapsakademiens. Handlingar* **24**, 1–39 (1898).

44. Ho, Y. S. & McKay, G. A Comparison of Chemisorption Kinetic Models Applied to Pollutant Removal on Various Sorbents. *Process Safety and Environmental Protection* **76**, 332–340 (1998).

45. Elovich, S. Y. & Larionov, O. G. Theory of adsorption from nonelectrolyte solutions on solid adsorbents. *Izv Akad Nauk SSSR* **11**, 198–203 (1962).

46. G. Ritchie, A. Alternative to the Elovich equation for the kinetics of adsorption of gases on solids. *Journal of the Chemical Society, Faraday Transactions 1: Physical Chemistry in Condensed Phases* **73**, 1650–1653 (1977).

47. Boyd, G. E., Adamson, A. W. & Myers, L. S. The Exchange Adsorption of Ions from Aqueous Solutions by Organic Zeolites. II. Kinetics1. *J. Am. Chem. Soc.* **69**, 2836–2848 (1947).

48. Weber, W. J. & Morris, J. C. Kinetics of adsorption on carbon from solutions. *J. Sanit. Eng. Div., Am. Soc. Civ. Eng.* **89**, 31–60 (1963).

49. Noh, J. S. & Schwarz, J. A. Estimation of surface ionization constants for amphoteric solids. *Journal of Colloid and Interface Science* **139**, 139–148 (1990).

50. Bandosz, T. J., Jagiello, Jacek. & Schwarz, J. A. Comparison of methods to assess surface acidic groups on activated carbons. *Anal. Chem.* **64**, 891–895 (1992).

51. Menéndez, J. A., Illán-Gómez, M. J., y León, C. A. L. & Radovic, L. R. On the difference between the isoelectric point and the point of zero charge of carbons. *Carbon* **33**, 1655–1657 (1995).

52. Karanfil, T. & Kilduff, J. E. Role of Granular Activated Carbon Surface Chemistry on the Adsorption of Organic Compounds. 1. Priority Pollutants. *Environ. Sci. Technol.* **33**, 3217–3224 (1999).

53. Popovicheva, O. *et al.* Water interaction with hydrophobic and hydrophilic soot particles. *Phys. Chem. Chem. Phys.* **10**, 2332–2344 (2008).

54. Liu, L. *et al.* Water adsorption on carbon - A review. *Advances in Colloid and Interface Science* **250**, 64–78 (2017).

55. Schwarzenbach, R. P., Gschwend, P. M. & Imboden, D. M. *Environmental Organic Chemistry*. (John Wiley & Sons, 2016).

56. Grahame, D. C. Diffuse Double Layer Theory for Electrolytes of Unsymmetrical Valence Types. *J. Chem. Phys.* **21**, 1054–1060 (1953).

57. Arrhenius, S. Über die Reaktionsgeschwindigkeit bei der Inversion von Rohrzucker durch Säuren. *Zeitschrift für Physikalische Chemie* **4U**, 226–248 (1889).

58. Ogram, A. V., Mathot, M. L., Harsh, J. B., Boyle, J. & Pettigrew, C. A. Effects of DNA Polymer Length on Its Adsorption to Soils. *Appl Environ Microbiol* **60**, 393–396 (1994).

59. Pietramellara, G., Franchi, M., Gallori, E. & Nannipieri, P. Effect of molecular characteristics of DNA on its adsorption and binding on homoionic montmorillonite and kaolinite. *Biol Fertil Soils* **33**, 402–409 (2001).

60. Pursell, C. J., Hartshorn, H., Ward, T., Chandler, B. D. & Boccuzzi, F. Application of the Temkin Model to the Adsorption of CO on Gold. *J. Phys. Chem. C* **115**, 23880–23892 (2011).

61. Franchi, M. *et al.* Clay-Nucleic Acid Complexes: Characteristics and Implications for the Preservation of Genetic Material in Primeval Habitats. *Orig Life Evol Biosph* **29**, 297–315 (1999).

62. Saeki, K., Kunito, T. & Sakai, M. Effects of pH, ionic strength, and solutes on DNA adsorption by andosols. *Biol Fertil Soils* **46**, 531–535 (2010).

63. Yaacobi, M. & Ben-Naim, A. Hydrophobic interaction in water-ethanol mixtures. *J Solution Chem* **2**, 425–443 (1973).

64. Ballal, D. & Chapman, W. G. Hydrophobic and hydrophilic interactions in aqueous mixtures of alcohols at a hydrophobic surface. *J. Chem. Phys.* **139**, 114706 (2013).

65. Herskovits, T. T. Nonaqueous solutions of DNA: Factors determining the stability of the helical configuration in solution. *Archives of Biochemistry and Biophysics* **97**, 474–484 (1962).